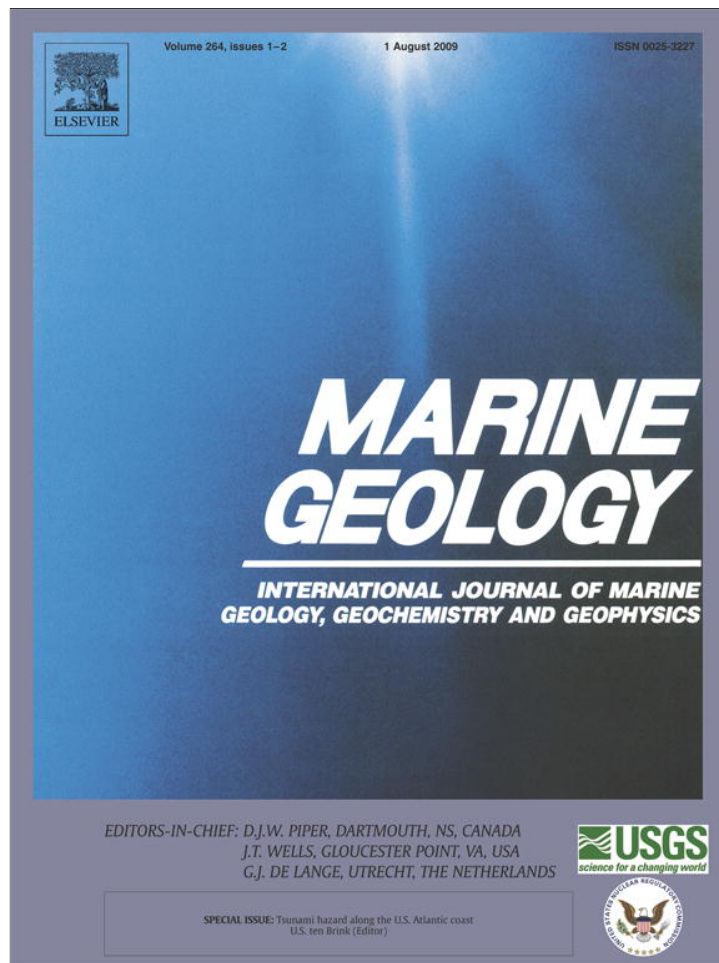


Provided for non-commercial research and education use.
Not for reproduction, distribution or commercial use.

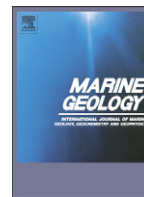


This article appeared in a journal published by Elsevier. The attached copy is furnished to the author for internal non-commercial research and education use, including for instruction at the authors institution and sharing with colleagues.

Other uses, including reproduction and distribution, or selling or licensing copies, or posting to personal, institutional or third party websites are prohibited.

In most cases authors are permitted to post their version of the article (e.g. in Word or Tex form) to their personal website or institutional repository. Authors requiring further information regarding Elsevier's archiving and manuscript policies are encouraged to visit:

<http://www.elsevier.com/copyright>



Assessment of tsunami hazard to the U.S. East Coast using relationships between submarine landslides and earthquakes

Uri S. ten Brink^{a,*}, Homa J. Lee^b, Eric L. Geist^b, David Twichell^a

^a USGS, Woods Hole Science Center, Woods Hole, MA, United States

^b USGS, Western Coastal and Marine Geology, Menlo Park, CA, United States

ARTICLE INFO

Article history:

Received 10 January 2008

Received in revised form 15 May 2008

Accepted 16 May 2008

Keywords:

submarine landslide

landslide tsunami

1929 Grand Banks earthquake

continental slope

slope stability

ABSTRACT

Submarine landslides along the continental slope of the U.S. Atlantic margin are potential sources for tsunamis along the U.S. East coast. The magnitude of potential tsunamis depends on the volume and location of the landslides, and tsunami frequency depends on their recurrence interval. However, the size and recurrence interval of submarine landslides along the U.S. Atlantic margin is poorly known. Well-studied landslide-generated tsunamis in other parts of the world have been shown to be associated with earthquakes. Because the size distribution and recurrence interval of earthquakes is generally better known than those for submarine landslides, we propose here to estimate the size and recurrence interval of submarine landslides from the size and recurrence interval of earthquakes in the near vicinity of the said landslides. To do so, we calculate maximum expected landslide size for a given earthquake magnitude, use recurrence interval of earthquakes to estimate recurrence interval of landslide, and assume a threshold landslide size that can generate a destructive tsunami. The maximum expected landslide size for a given earthquake magnitude is calculated in 3 ways: by slope stability analysis for catastrophic slope failure on the Atlantic continental margin, by using land-based compilation of maximum observed distance from earthquake to liquefaction, and by using land-based compilation of maximum observed area of earthquake-induced landslides. We find that the calculated distances and failure areas from the slope stability analysis is similar or slightly smaller than the maximum triggering distances and failure areas in subaerial observations. The results from all three methods compare well with the slope failure observations of the $M_w = 7.2$, 1929 Grand Banks earthquake, the only historical tsunamigenic earthquake along the North American Atlantic margin. The results further suggest that a $M_w = 7.5$ earthquake (the largest expected earthquake in the eastern U.S.) must be located offshore and within 100 km of the continental slope to induce a catastrophic slope failure. Thus, a repeat of the 1755 Cape Anne and 1881 Charleston earthquakes are not expected to cause landslides on the continental slope. The observed rate of seismicity offshore the U. S. Atlantic coast is very low with the exception of New England, where some microseismicity is observed. An extrapolation of annual strain rates from the Canadian Atlantic continental margin suggests that the New England margin may experience the equivalent of a magnitude 7 earthquake on average every 600–3000 yr. A minimum triggering earthquake magnitude of 5.5 is suggested for a sufficiently large submarine failure to generate a devastating tsunami and only if the epicenter is located within the continental slope.

Published by Elsevier B.V.

1. Introduction

Recent tsunamigenic landslides (e.g., Papua New Guinea, Tappin et al., 2001) and re-analysis of historical tsunamis (e.g., the 1918 western Puerto Rico, Lopez et al., 2008) have contributed to the realization that landslides can locally generate high-amplitude tsunamis. Along the Atlantic margin, a landslide-generated tsunami in 1929 resulted in loss of life and property along the Newfoundland coast (e.g., Piper and Aksu, 1987; Fine et al., 2005). The U.S. Atlantic coast is particularly vulnerable to devastation from tsunamis because of the high density of population

and infrastructure along its low-lying coastal areas and estuaries. Seafloor observations show large landslide scars and debris fields on the continental slope (e.g., Booth et al., 1993; Chaytor et al., 2007; Twichell et al., 2009). Evaluation of the spatial and temporal distributions of submarine landslides should therefore help estimate the probability of landslides; however, it is sometimes difficult to determine whether each of the scars and debris fields represents single or composite landslides (Twichell et al., 2009), and the ages of the slope failures are often not well-constrained (Lee, 2009). To overcome the paucity of knowledge about the spatial and temporal distributions of landslides along the U.S. continental slope, we propose here an indirect approach. The approach is to derive relationships between the sizes of submarine landslides and earthquakes and use published earthquake recurrence

* Corresponding author.

E-mail address: utenbrink@usgs.gov (U.S. ten Brink).

intervals to estimate the maximum sizes of submarine landslides and their recurrence. The minimum landslide size that can cause a devastating tsunami can be estimated from tsunami runup models of selected landslides of different sizes along the margin. While this approach does not accurately provide the size of individual landslides, it provides an upper bound to the landslide size and to the probability of recurrence of tsunamigenic landslides. We focus here on the relationship between earthquakes and submarine landslides, because, although other triggering mechanisms have been proposed for submarine landslides (e.g., gas hydrate dissociation, excess pore pressure, salt movement; see Lee, 2009), to date, observed landslide-generated tsunamis have all been triggered by earthquakes.

Three methods to derive the relationship between submarine landslides and earthquakes are presented. The first method, which is introduced in Sections 2 and 3, is based on slope stability analysis. The other two, which are introduced in Section 4, are based on subaerial analogs. In Section 4 we compare between the three methods, and compare the predictions based on these methods to the only historical earthquake-generated landslide along the Atlantic coast, namely the 1929 Grand Banks. In Section 5, we estimate the minimum earthquake magnitude that could cause a devastating tsunami (i.e., one that will overtop a barrier island or a sand berm) resulting from a submarine landslide. In Section 6, we extrapolate earthquake recurrence rates for the Canadian margin to the U.S. margin, and define the region, where earthquakes could induce large landslides. This approach may help estimate the potential for landslide-generated tsunamis along the U.S. Atlantic margin.

2. Slope stability

The first method to relate earthquake magnitude to the distance from the ruptured fault to the submarine failure (henceforth, fault-to-failure distance) and to the landslide area, is presented in the next two sections. The method is based on calculating catastrophic slope failure conditions due to horizontal acceleration by earthquakes. By catastrophic failure we mean a failure that causes downhill mass movement of a finite distance. In engineering literature, finite distance is taken to be at least 1 m (e.g., Newmark, 1965; Hynes-Griffin and Franklin, 1984), which is assumed to be sufficient for continued downhill movement.

2.1. Methodology

We assume that earthquake-induced landslides, at least in soft sediments, may occur when the shear stress τ on a slip surface exceeds the undrained shear strength S_u of the sediment (e.g., Morgenstern, 1967). This condition is expressed as

$$F = S_u / \tau \leq 1 \quad (1)$$

where F is known as the Factor of Safety.

The downslope shear stress in a pseudo-static representation consists of the downslope component of gravitational stress added to a pseudo-static horizontal stress related to earthquake loading (Morgenstern, 1967).

$$\tau = \gamma' z \sin \beta \cos \beta + k \gamma z \cos^2 \beta \quad (2)$$

where γ' is the submerged (buoyant) unit weight in an infinite slope with an angle β , k denotes the horizontal acceleration due to an earthquake (as a fraction of the gravitational acceleration), z represents the vertical thickness of the landslide, and γ is the unit total weight of the slide.

Setting $F = 1$ as the failure condition yields:

$$S_u / (\gamma' z) = \cos \beta \sin \beta + k(\gamma / \gamma') \cos^2 \beta. \quad (3)$$

The ratio $S_u / (\gamma' z)$ is defined as the c/p ratio and can be measured in the laboratory by subjecting samples to cyclic loading in triaxial tests and observing their failure (e.g., Seed and Lee, 1966; Lee et al., 2000). Rearranging Eq. (3), the critical acceleration, corresponding to the earthquake acceleration k_y , at which the pseudo-static stress just equals the shear strength, is:

$$k_y = (c/p)(\gamma' / \gamma) / (\cos^2 \beta) - (\gamma' / \gamma) \tan \beta. \quad (4)$$

In other words, the peak earthquake acceleration has to be equal to or exceed k_y , to overcome the shear strength of the sediment.

However, the failure condition will lead to a catastrophic slope failure only if the shaking causes the slope to be displaced a finite distance (Newmark, 1965). A catastrophic slope failure will be affected not only by the pseudo-static condition (1), but also by the cyclic nature of earthquake acceleration and its duration. During an earthquake, the ground seldom experiences maximum acceleration in the direction of slope failure. The resultant response may be non-linear and dependent on a transient buildup of pore pressure (Newmark, 1965), the magnitude of shaking (Makdisi and Seed, 1978) and on variations of shaking with depth (Cetin et al., 2004). Model tests (Newmark, 1965; Makdisi and Seed, 1978) have shown that the peak earthquake acceleration necessary to cause a catastrophic displacement must be much larger than the undrained shear strength.

Empirical and hybrid empirical attenuation relationships for the horizontal component of peak spectral acceleration (PSA) have been derived using databases of hundreds of accelerograms (Abrahamson and Silva, 1997, and references therein). For eastern North America, these relationships take the general form of

$$\ln Y = c + f_1(M) + f_2(M, r) + f_3(r), \quad (5)$$

(Campbell, 2003), where Y is the 5% damped peak spectral acceleration (PSA), M is the moment magnitude, r is the distance from the fault to the site, c is a constant, and f is a function.

2.2. Selection of parameters

The c/p ratio was measured in samples from a 38 m deep hole at water depth of 639 m on the Hudson Apron offshore New Jersey (Locat et al., 2003). The c/p ratio decreases from 0.5 near the surface to ≤ 0.2 at depths greater than 10 m, and is 0.15 at the base of the hole (Locat et al., 2003). Based on a compilation of 106 landslides along the U.S. Atlantic slope, the relationship between landslide volume V and area A is found to be $V = 0.0163 A^{1.1}$ (Chaytor et al., 2009), suggesting that the average landslide thickness is ~ 16 m. Therefore, the slide plane depth is likely to be greater than 10 m, justifying the use of $c/p = 0.2$. The relatively low value of c/p may indicate sediment overpressure or the presence of aquifers, which were suggested for the New Jersey margin (Dugan and Fleming, 2000). However, in the absence of direct measurements of pore pressure and cyclic loading measurements of the cored sediments, it is possible that the low c/p values represent coring disturbance. We therefore also calculated the potential slope failure with a more typical c/p value of 0.3. A soil density of 1600 kg/m^3 was measured in this hole (Locat et al., 2003), resulting in a weight ratio, $\gamma' / \gamma = 0.375$.

The ratio of the critical acceleration necessary to induce catastrophic displacement (taken as 1 m) k_y to the peak spectral acceleration K_{PSA} was calculated by a sliding block analysis for 348 horizontal-component records from earthquakes in California and was found to be $k_y / K_{PSA} = 0.17$ (Hynes-Griffin and Franklin, 1984). By comparing observations of landslide scarps offshore California to peak seismic acceleration from shake maps and equating a catastrophic failure with a displacement of at least 1 m, Lee et al. (2000) derived a ratio of $k_y / K_{PSA} \leq 0.15$. Similar empirical relationships have so far not

been derived for the U.S. Atlantic continental margin. We therefore use $k_y/K_{PSA} = 0.15$ in our calculations.

We calculate PSA using Campbell's (2003) hybrid empirical ground motion attenuation relationships for hard rock in eastern North America. In contrast to the western U.S., this attenuation model is not completely empirical because of the paucity of large earthquakes in the eastern North America. There is no previous guidance for the choice of the fundamental period of shaking. For a soil layer with constant velocity and density, the fundamental period T depends on the layer thickness H , and the shear wave velocity V_s :

$$T = 4H / V_s \quad (6)$$

(Dorby et al., 1976).

Shallow (<100 m) Pliocene and Quaternary marine sediments on the New Jersey shelf have a shear wave velocity of 200–400 m/s (Ewing et al., 1992), and the thickness of the sliding layer is typically 20–100 m. Hence, T may vary between 0.2 and 2.0 s, and we choose $T = \sim 0.75$ s as an average estimate.

The expected site amplification in shallow (top 30 m) soft sediments with $V_s = 310$ m/s relative to hard rock sites ($V_s = 2800$ m/s) is ≥ 3.5 (Boore and Joyner, 1997). Hynes-Griffin and Franklin (1984) derived an amplification factor of approximately 3. Consequently, we multiply the calculated peak spectral acceleration by 3.5 to account for site amplification.

3. Results of slope stability analysis

3.1. Maximum distance to failure

The calculated maximum distance r_{max} from a rupturing fault to sites where submarine slope failure is expected is that distance at which the modified peak spectral acceleration of the earthquake, k_{PSA} , is equal or smaller than the critical acceleration, necessary to cause catastrophic displacement, k_y ,

$$0.15 \times 3.5 \times K_{PSA(T=0.75)} \leq k_y. \quad (7)$$

This distance increases with seabed slope angle and earthquake magnitude (Fig. 1a). The distance is larger for $c/p = 0.2$ than for $c/p = 0.3$ (compare Fig. 1a and c), but does not exceed 62 km for slopes $\leq 2^\circ$, and 102 km for slopes $\leq 6^\circ$ even for an earthquake with a magnitude $M_w = 7.5$. Following Frankel et al. (1996) and Mazzotti and Adams (2005), we used $M_w = 7.5$ as the estimated largest expected event along the U.S. Atlantic coast. Except along canyon walls and on the flanks of seamounts, the lower continental slope and continental rise have slopes $< 2^\circ$ (Fig. 3).

Based on the results in Fig. 1a, an $M7.5$ earthquakes occurring inland from the Atlantic coast are unlikely to cause sediment failure on the continental slope because of the great distance (>100 km) between them. Therefore, historical earthquakes such as the 1888

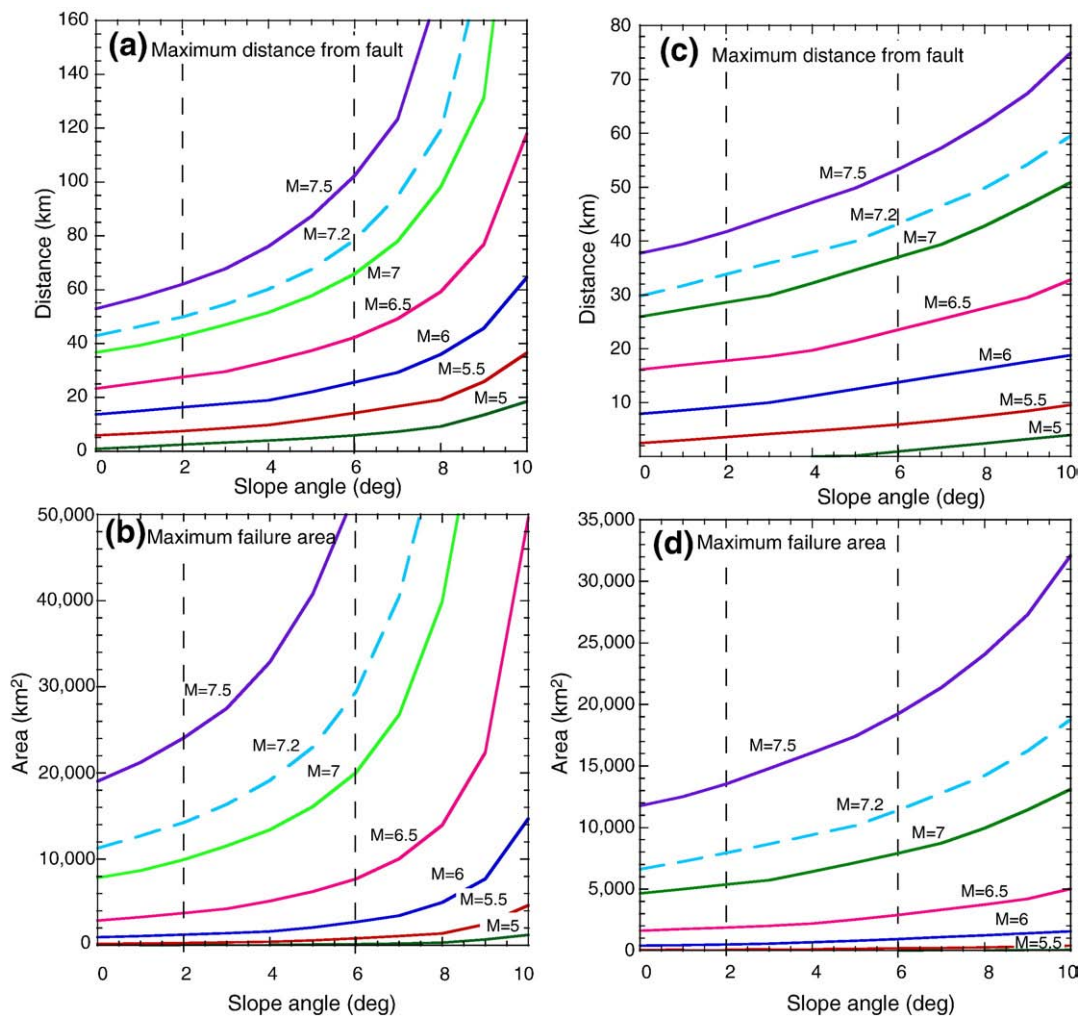


Fig. 1. (a) Calculated maximum distance from a fault to sites where failure is expected, as a function of slope angle and earthquake moment magnitude. The following parameters were used: $c/p = 0.2$, $k_y/K_{PSA} = 0.15$, $\gamma/\gamma' = 0.375$, and peak seismic acceleration (PSA) relationship of Campbell (2003) for $T = 0.75$ s. Vertical dashed lines mark 2° and 6° (b) Calculated maximum failure area as a function of slope angle and earthquake moment magnitude using the same parameters as in (a). (c) Same as (a) with $c/p = 0.3$. (d) Same as (b) with $c/p = 0.3$.

Charleston and 1755 Cape Ann earthquakes (Fig. 2) would not have caused a slope failure on the continental slope. The only exception could be the area around Cape Hatteras where the shelf is 50 km wide (Fig. 2). An $M7.5$ earthquake located up to 102 km from the upper slope could cause failure on slopes of 6° , but such high slope angles are confined to only small portions of the continental margin (Fig. 3). Failures on the more typical slopes of 2° require the epicenter to be within 62 km of the shelf edge. An $M6.5$ earthquake could cause a landslide only if located within 28 km of the continental slope of 2° and within 42 km of a 6° slope and an $M5.5$ only if located within 7 and 14 km, respectively.

Mosher et al. (1994) have arrived at a similar conclusion from their geotechnical analysis of cores from landslides on the Scotian shelf, namely, that an earthquake would have to be local to generate sufficient ground acceleration for slope failure. Their calculated distance to failure, however, was larger than derived here (40 km for $M5$ and 100 km for $M6.7$; Mosher et al., 1994) probably because catastrophic failure was not factored in their analysis.

Note that a finite distance to failure is predicted even on flat ground $\beta=0^\circ$. Sediment strength will decline with continued shaking, but in the absence of a slope, the weakened sediments will not move appreciably.

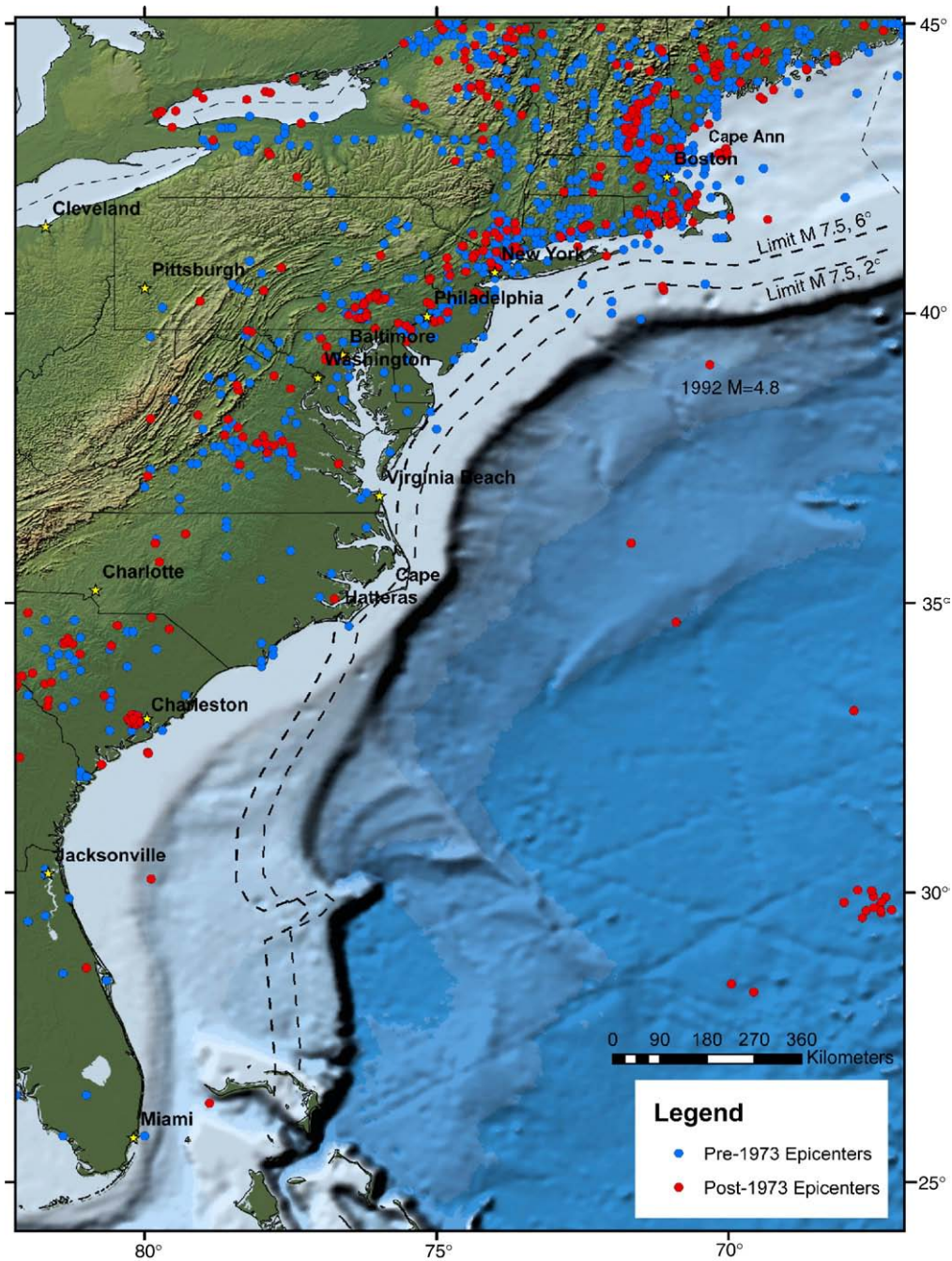


Fig. 2. Earthquake epicenters along the U.S. Atlantic coast from the NEIC catalog (<http://neic.usgs.gov/neis/epic/epic.html>). Blue dots – earthquakes between 1534 and 1973. Red dots – earthquakes post-1973 catalog. Dashed lines – distances of 62 and 102 km from the top of the continental slope. These are the maximum predicted distances based on slope stability analysis, for an $M7.5$ earthquake, to cause a catastrophic failure of the continental slope with slope angles of 2° and 6° , respectively. Smaller magnitude earthquakes will have to be located closer to the continental slope to cause catastrophic slope failures.

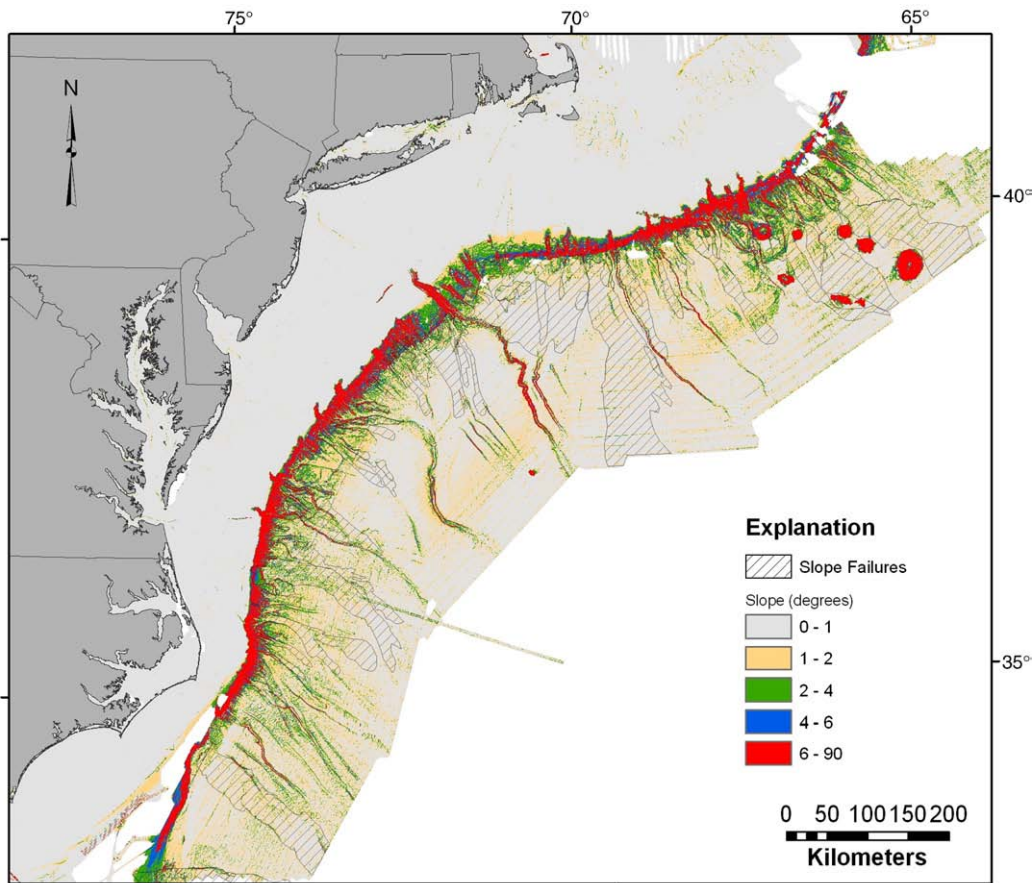


Fig. 3. Slope angle of the U.S. Atlantic continental margin and overlays of interpreted slope failures (Twichell et al., 2009).

3.2. Maximum slope failure area

The maximum slope failure area A_L can be calculated by assuming that the area is defined by the maximum distance to failure, r_{max} . Hence, the maximum failure area is a rectangle containing the fault trace, whose length is the fault length L and whose half-width is r_{max} , plus two half circles with a radius r_{max} at either end of the fault (Fig. 4a), as given by:

$$A_L = \pi r_{max}^2 + L \cdot 2r_{max} \quad (8)$$

The fault length as a function of magnitude is given by the empirical relationship

$$\log(L) = -2.44 + 0.59M \quad (9)$$

(Wells and Coppersmith, 1994).

The maximum failure area reaches 24,100 km² for slope angles <2° and $M=7.5$ (Fig. 1b). The maximum slope failure area refers to an “ideal” position of a fault within the slope area and parallel to its strike, in which case the fault lengths L in Eqs. (8) and (9) are the same. The expected failure area will be smaller if the fault is not parallel to the margin and/or if the fault is located on the shelf or in the abyssal plain (Fig. 4b). Note that we assume no catastrophic failure on the shelf, where the slope is ~0°.

Slope angles >2° along the Atlantic coast of the U.S. are generally limited to a <30 km wide zone of the upper slope as well as some submarine canyons (Fig. 3). Hence, failure area will likely deviate from the simple shape in Eq. (8), such that a longer portion of the steep upper slope will fail during an earthquake, compared to the lower slope (Fig. 4b). The maximum total failure area will therefore be slightly larger than that for a 2° slope. For example, for an $M7.2$

earthquake, the total area will be about 15,900 km² instead of 14,200 km² due to the added contribution of the upper slope. The maximum observed landslide area along the Atlantic margin is 15,240 km² and is located off southern New England (Twichell et al., 2009).

3.3. Comparison with the 1929 Grand Banks landslide

The modeling results can be compared with observations of the 1929 Grand Banks landslide, that caused the only historical tsunami along the Atlantic margin of North America. On the basis of the area encompassing the instantaneous breaks of communication cables along the sea floor during the earthquake, Piper et al. (1985) and Mosher and Piper (2007) estimated the region where at least 10% of the sea floor failed to be 22,700 km². Using side-scan sonar they estimated the region where 100% of the sea floor failed to be 7200 km². Piper and Aksu (1987) and Piper et al. (1999) estimated the

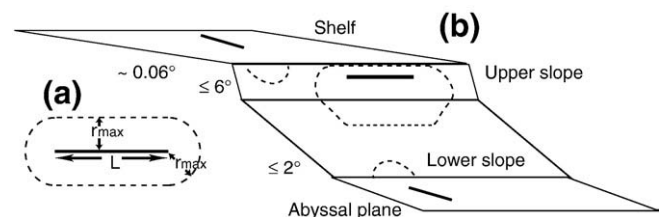


Fig. 4. (a) Schematic diagram showing the geometry of a slope failure, including fault length L , maximum distance from fault to failure r_{max} , and maximum failure area (dashed line). (b) Schematic diagram of the continental margin. Heavy lines – different fault orientations with dashed lines enclosing their associated maximum failure areas.

average failure thickness as 20 m and the volume of failed material to be > 150 km³. McCall et al. (2005) estimated the total volume of failed material in the area of 100% seafloor failure to be 93.5 km³. Hughes Clarke et al. (1990) pointed out that a small volume of debris flow (<15 km³) appears to post-date the turbidity flow, and could have been triggered by aftershocks.

The $M_w = 7.2 \pm 0.3$ 1929 Grand Banks earthquake was located in the middle of the steep upper slope (Bent, 1995). For a 2° average slope and c/p ratio of 0.2, the predicted area of the entire possible failure region from an $M7.2$ earthquake, is 14,200 km² (Fig. 1b). With a 30-km-wide steeper (6°) upper slope replacing part of the predicted failure area of a 2° slope, the total predicted maximum failure is 15,900 km². This value is similar to the observed slide failure area associated with the 1929 earthquake within the uncertainties of the model parameters, the earthquake magnitude and the observations of the failure area. (For example, the predicted area from $M7.5$ earthquake is 24,100 km²; Fig. 5b). The ~30 km wide upper slope is steeper (~6°), hence a longer part of the upper slope is expected to fail along strike compared to the less steep lower slope (Fig. 4b). The region with 100% failure indeed extends along 210 km of the upper slope, whereas the length of lower slope failure is half of that (Mosher and Piper, 2007). The area with at least 10% sea floor failure has a maximum failure length of 245 km in the upper slope and is also narrower on the lower slope (Piper et al., 1985; Mosher and Piper, 2007). The calculated length of upper slope failure for $M7.2$ is 200 km, which is within the observed estimates.

3.4. Additional notes

The choice of attenuation relationship also affects the prediction of seismic acceleration. Using different attenuation relationships for eastern North America (Tavakoli and Pezeshk, 2005), the predicted distance to failure and slope failure area are slightly larger than those predicted by Campbell's (2003) relationships (Fig. 5). The difference becomes considerably larger for large magnitude earthquakes ($M7$), because of changes in the functional relationship of Tavakoli and Pezeshk (2005) at distances of 70 and 130 km.

Predictions of landslide susceptibility were made for two regions offshore California by coupling slope stability analysis with the predicted peak seismic acceleration (Lee et al., 2000). Published maps of peak seismic acceleration with 10% probability of exceedance in the next 50 yr were used to estimate the peak ground acceleration along the margin (Lee et al., 2000). The California continental slope is generally much closer to land than the Atlantic continental slope of the U.S., and the frequency of earthquakes is much higher; therefore the use of such maps is justified there. Peak acceleration maps of the U.S. Atlantic coast (Fig. 12 of Frankel et al., 1996) do not extend into the continental margin and are heavily skewed at the 50-year exposure time toward the two large historical earthquakes in the U.S. East Coast – Cape Ann (1755) and Charleston (1888). Hence, we had to infer the seismic acceleration directly from the maximum magnitude (M_{max}) of hypothetical earthquakes, with the intention of calculating the probability of occurrence of earthquakes of certain magnitude along the margin in the future. At present, however, microseismicity monitoring along the continental margin ($\leq M3.5$) is incomplete due to the lack of dense instrument coverage, the large distance from shore, and the relatively short measurement period in comparison to rates of seismic moment release.

4. Other methods – Using land-based empirical relationships

Empirical estimates of landslide effects due to earthquakes have been carried out on land, where these effects can be easily observed and surveyed (Keefer, 1984; Ambraseys, 1988; Rodriguez et al., 1999; Keefer, 2002), and references therein). Ambraseys (1988) proposed a

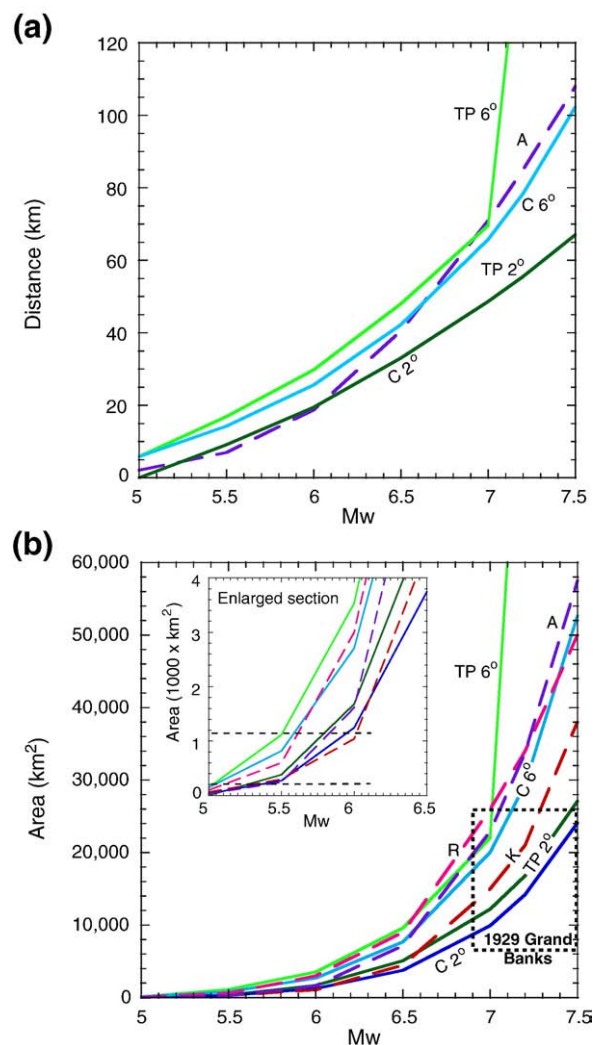


Fig. 5. (a) Comparison between three methods to derive relationship between earthquakes and submarine landslides. Two parameters are compared as a function of earthquake magnitude: (a) maximum distance to slope failure from fault rupture, and (b) maximum area of slope failure. Methods to derive maximum area of slope failure are compared to the observed 1929 Grand Banks landslide, with the uncertainty in area and magnitude shown as a dashed rectangle. Solid curves were calculated by the slope stability analysis method for seabed slopes of 2° and 6° with the PSA relationships of Campbell (2003) (C2° and C6°) and Tavakoli and Pezeshk (2005) (TP2° and TP6°). Dashed curves are empirical relationships of maximum distance to liquefaction on land, A (Ambraseys, 1988), and observed maximum failure area on land, K (Keefer, 1984) and R (Rodriguez et al., 1999). Also shown in (b) is a curve (marked A) of the expected maximum failure area using Ambraseys' (1988) empirical relationship for maximum distance to liquefaction. Inset shows enlargement of maximum failure area as a function of earthquake magnitude for low magnitudes. Horizontal dashed lines in inset mark the areas of two submarine slides within the Currituck slide complex, the larger area is expected to cause a destructive tsunami and the smaller one is not. See text for further explanations.

curve that bounds the maximum distances from the fault rupture to liquefaction sites, which we call the maximum liquefaction distance r_{liq} :

$$M_w = 0.18 + 9.2 \cdot 10^{-8} r_{liq} + 0.9 \log(r_{liq}). \quad (10)$$

Liquefaction on land is indicative of catastrophic soil failure in the absence of a topographic slope and in the presence of a water table close to the surface. Hence, these observations can probably be compared to the distance of failure of submarine sediments from the triggering fault, predicted by slope stability analysis, because of the generally low submarine slopes (Fig. 5a). The maximum observed liquefaction distance falls within the predicted distance from slope

stability analysis for slopes between 2° and 6° and $c/p=0.2$, but is higher than the predicted distance from slope stability analysis for $c/p=0.3$ (Fig. 5a).

Based on post-earthquake observations, Keefer (1984) and Rodriguez et al. (1999) defined an upper bound curve for the total area in which earthquake-triggered landslides occur (Fig. 5b). Their compilations of landslide areas do not differentiate between different slope angles or landslide types, such as rock falls, disrupted and coherent rock slides, soil spreads, and flows. As with maximum distance to failure, the area calculated from slope stability analysis for slopes between 2° and 6° is similar to or slightly less than Keefer (1984) and Rodriguez et al. (1999) curves. An expected maximum failure area can also be calculated by combining the maximum observed distance from the fault r_{liq} to liquefaction (cf. Eq. (10), Ambraseys, 1988) and Eq. (9). The expected maximum failure area from the maximum distance to liquefaction (A in Fig. 5b) appears to be similar to the observed maximum landslide area by Rodriguez et al. (1999, R in Fig. 5b).

The maximum subaerial failure area resulting from an $M_{7.2}$ earthquake is between 21,000 km² (when using Keefer, 1984, relationship) and 36,000 km² (when using Rodriguez et al., 1999, relationship), and the maximum area using the liquefaction distance is 33,800 km². These estimates are within, or larger than, observed failure area of the 1929 Grand Banks landslide ($M_w=7.2\pm 0.3$, area = 7200–22,700 km², Fig. 5b).

At present, it is unclear whether the use of slope stability analysis or the subaerial observations is the more valid method for estimating the relationship between earthquakes and submarine landslides. The empirical relationships of Ambraseys (1988), Keefer (1984), and Rodriguez et al. (1999) are based on observations from around the world, with variable drainage conditions, slope direction and angle, and lithology within a single affected area, whereas the slope stability analysis uses a specific attenuation relationship for the U.S. East Coast, a monotonous and fairly low slope, and observed geotechnical parameters for the Atlantic continental slope. However, the PSA may not account for the duration of shaking, which increases with magnitude. In addition, the ratio of the peak spectral acceleration K_{PSA} to the acceleration k_y necessary to induce catastrophic displacement (taken as 1 m) was assumed here to be constant (Hynes-Griffin and Franklin, 1984), but it may in fact increase with magnitude (Makdisi and Seed, 1978). One way to explicitly account for the increase in the duration of shaking is by using Arias intensity instead of PSA. The Arias intensity is the integral of the acceleration–time history (Travasarou et al., 2003, and references therein). However, an Arias intensity relationship for the eastern U.S. has not yet been developed.

5. Magnitude threshold for devastating tsunamis

The morphology of the U.S. East Coast is variable with many coastlines having sand berms or barrier islands. Detailed LIDAR elevation maps of the coast stretching from North Carolina to southern Florida show that elevations typically vary from 2–8 m above the NAVD88 88 reference level (Elko et al., 2002). The NAVD88 reference level is on average 0.5–1.25 m below the mean highest high water level (Weber et al., 2005) hence this amount has to be subtracted from the dune height in a worst-case scenario. Similar detailed information of dune height or of a maximum elevation close to shore is lacking north of North Carolina. Hydrodynamic modeling shows that a tsunami can overtop a sand dune or barrier island even if the tsunami's wave amplitude is lower than the sand dune elevation (Geist et al., 2009–this volume, their Fig. 12) because of the large wavelength of the tsunami relative to that of the sand dune. Tsunami wave amplitude from the 1929 Grand Banks tsunami was estimated at 3–8 and the maximum runup was 13 m (Fine et al., 2005). Recognizing that dune elevation is highly variable in space, we assume in this analysis a tsunami with wave height of 2 m offshore, as one that can overtop many of the dunes and can therefore be potentially damaging.

The maximum calculated area of slope failure is sufficiently large for earthquakes magnitudes greater than $M=5.5$ –6 to cause a devastating tsunami (inset in Fig. 5) if the epicenter is optimally located at the base of the upper slope and if the entire area indeed fails. This estimate is based on the calculated wave amplitude at 22 m water depth from hydrodynamic modeling of the Currituck slide offshore Virginia (Geist et al., 2009–this volume). The modeling suggests that, for the particular characteristics of the Currituck region and for a near-shore bottom friction of 0.25 – 1×10^{-2} , a failure area of 300 km² would generate a wave amplitude of 1.6–2.4 m, which is probably not enough to cause a devastating tsunami, but a failure area of 1240 km² would generate a wave amplitude of 2–4.5 m, which could overtop the sand berms (inset in Fig. 5; Geist et al., 2009–this volume). A larger earthquake magnitude may be necessary to cause a devastating tsunami from a submarine landslide along the southern New England margin, because the shelf there is twice as wide as the 80-km-wide Currituck shelf. The amplitude of tsunami waves is expected to decay as they travel over the shelf because of bottom friction and dispersion, the latter caused by the long propagation time across the shallow shelf. At present, there are no hydrodynamic models for this region.

6. Probability of earthquake recurrence

Analysis of the rates of deformation in eastern Canada (Mazzotti and Adams, 2005) suggests that the continental slope of eastern Canada from the Arctic to Georges Bank is associated with a relatively high average annual seismic moment release (2 – 10×10^{17} N M/yr) for an intraplate setting. The annual moment release is the equivalent of an M_w7 earthquake occurring somewhere along this ~ 6000 km long margin every 40–200 yr. The source of the seismicity is unclear but some workers have suggested that seismicity is due to glacial unloading of the Laurentide ice sheet (Mazzotti and Adams, 2005, and references therein). Seismicity offshore the U.S. Atlantic coast is mostly concentrated offshore New England (Fig. 3), the only sector to have undergone glacial unloading. It is possible therefore that the same seismic regime present on the eastern Canadian margin extends from the Canadian continental slope south along the 400-km-long New England margin. Using Canadian seismicity as a guide and assuming equal probability for the spatial distribution of earthquakes (e.g., Swafford and Stein, 2007), the rate of seismic moment release along the New England margin is 1/15 that of the Canadian estimate, which is equivalent to an $M=7.0$ earthquake occurring every 600–3000 yr. However, the frequency of submarine landslide-induced destructive tsunamis is likely smaller than this because of additional conditions such as optimally located epicenter within the vulnerable area, catastrophic failure of much of the vulnerable area, and rapid slide movement, that are necessary to generate a destructive tsunami.

South of the New England margin, the seismicity rate appears lower than to the north (Fig. 2). Nevertheless, possible faults have been identified on the slope south of the Cape Fear area (Hornbach et al., 2007) and south of the Currituck slide (Locat et al., 2009). These faults may be related to salt movement at depth and may be associated with the slides (Hornbach et al., 2007). The recurrence interval on these faults is unknown.

7. Conclusions

It is clear from the analysis above that there are large uncertainties in estimating tsunami probability with this approach. These uncertainties are attributed to the choice of the spectral acceleration period, the amplification due to soft sediments, the choice of c/p , sediment thickness, the presence of overpressured or liquefiable sediments, and the recurrence interval of seismicity. Likewise, the applicability of land-based empirical relationship of heterogeneous lithologies and

slopes to submarine slopes has not been established. Nevertheless, the fit of the predictions of landslide area from magnitudes of earthquakes for all three methods to the observed area of the 1929 Grand Banks landslide is encouraging, keeping in mind that this is a single example, and the total area of the Grand Banks slide is still not well-constrained. With these uncertainties in mind, we can reach several conclusions:

- (a) Slope stability analysis suggests that the upper slope of the continental margin (slope angle $\leq 6^\circ$) will be affected by earthquakes with magnitudes of 5.5, 6.5, and 7.5, only if the earthquakes occur at distances less than 14, 42, and 102 km from the upper slope, respectively. For the lower, more shallowly dipping slope ($\leq 2^\circ$), the distances are much smaller (i.e., 7, 28, and 62 km, respectively). These distances represent maximum distances and will be smaller if $c/p = 0.3$ is assumed in the analysis. This analysis suggests that, with the exception of Cape Hatteras, only offshore earthquakes may be able to trigger submarine landslide-generated tsunamis.
- (b) The maximum calculated area of slope failure is sufficiently large for earthquakes with magnitude greater than $M5.5$ to cause a devastating tsunami if the epicenter is optimally located at the base of the upper slope and if the entire area indeed fails.
- (c) Based on extrapolation of results from the Canadian margin, the rate of release of seismic moment along the New England margin is estimated to be equivalent to an $M7.0$ earthquake occurring every 600–3000 yr. If these earthquakes are located at the base of the upper slope so as to maximize the failure area, or if slope sediments are overpressured, the resultant landslide area (and volume) will be sufficient to cause a destructive tsunami. The paucity of earthquakes south of the New England margin suggest that landslides there are either less frequent or they are generated by other mechanisms.
- (d) Slope stability analysis predicts similar or smaller maximum distance from fault to failure and maximum failure area than compilations of subaerial landslides and liquefactions. Both predictions from slope stability analysis and the extrapolation from land compilations fit the observations of the 1929 Grand Banks event, but other events are needed to validate these methods.

In summary, mapping entire continental margins and determining the age of submarine landslides is difficult and costly. We present here an approach to estimate the maximum size and recurrence interval of potentially-tsunamigenic submarine landslides from the size and recurrence interval of earthquakes in the near vicinity of the said landslides. We also suggest that the minimum landslide size that will cause a devastating tsunami can be estimated from tsunami runup models of selected landslides of different sizes. This information can help in the design of infrastructure facilities to withstand the effects of tsunamis. A successful implementation of this approach may require improvement in the seismic monitoring of continental margins.

Acknowledgements

Work funded by U.S.-NRC grant N6480 *Physical study of tsunami sources*. Discussions with Rob Kayen and Annie Kamerrer and helpful reviews by Carolyn Ruppel, Brian Collins, David Mosher, and Dave Tappin are gratefully acknowledged.

References

Abrahamson, N.A., Silva, W.J., 1997. Empirical response spectral attenuation relations for shallow crustal earthquakes. *Seismol. Res. Lett.* 68, 94–127.
 Ambraseys, N.N., 1988. Engineering seismology. *Earthq. Eng. Struct. Dyn.* 17, 1–105.
 Bent, A.L., 1995. A complex double-couple source mechanism for the Ms 7.2 1929 Grand Banks earthquake. *Bull. Seismol. Soc. Am.* 85, 1003–1020.
 Boore, D.M., Joyner, W.B., 1997. Site amplifications for generic rock sites. *Bull. Seismol. Soc. Am.* 87, 327–341.

Booth, J.S., O'Leary, D.W., Popenoe, P., Danforth, W.W., 1993. U.S. Atlantic continental slope landslides; their distribution, general attributes, and implications. In: Lee, H.J., Schwab, W.C., Twichell, D.C. (Eds.), *Submarine Landslides, Selected Studies in the U.S. Exclusive Economic Zone*. U.S. Geological Survey Bulletin, pp. 14–22.
 Campbell, K.W., 2003. Prediction of strong ground motion using the hybrid empirical method and its use in development of ground-motion (attenuation) relations in Eastern North America. *Bull. Seismol. Soc. Am.* 93, 1012–1033.
 Cetin, K.O., et al., 2004. Standard penetration test-based probabilistic and deterministic assessment of seismic soil liquefaction potential. *J. Geotech. Geoenviron. Eng.* 130, 1314–1340.
 Chaytor, J.D., Twichell, D.C., ten Brink, U.S., Buczkowski, B.J., Andrews, B.D., 2007. Revisiting submarine mass movements along the U.S. Atlantic continental margin, implications for tsunami hazards. In: Lykousis, V., Sakellariou, D., Locat, J. (Eds.), *Submarine Mass Movements and Their Consequences*. Springer, Dordrecht, pp. 395–403.
 Chaytor, J.D., ten Brink, U.S., Solow, A.R., Andrews, B.D., 2009. Size distribution of submarine landslides along the U.S. Atlantic margin. *Mar. Geol.* 264, 16–27.
 Dorby, R., Oweis, I., Urzua, A., 1976. Simplified procedures for estimating the fundamental period of a soil profile. *Bull. Seismol. Soc. Am.* 66, 1293–1321.
 Dugan, B., Fleming, P.B., 2000. Overpressure and fluid flow in the New Jersey continental slope: implications for slope failures and cold seeps. *Science* 289, 288–291.
 Elko, N.A., Sallenger, A.H., Jr., Guy, K., Morgan, K.L.M., 2002. Barrier island elevations relevant to potential storm impacts; 2, South Atlantic. USGS OF 02-0288.
 Ewing, J.L., Carter, J.A., Sutton, G.H., Barstow, N., 1992. Shallow water sediment properties derived from high-frequency shear and interface waves. *J. Geophys. Res.* 97, 4739–4762.
 Fine, I.V., Rabinovich, A.B., Bornhold, B.D., Thomson, R.E., Kulikov, E.A., 2005. The Grand Banks landslide-generated tsunami of November 18, 1929; preliminary analysis and numerical modeling. *Mar. Geol.* 215, 45–57.
 Frankel, A.D., Mueller, C.S., Barnhard, T.P., Perkins, D.M., Leyendecker, E.V., Dickman, N. et al., 1996. National seismic-hazard maps; documentation June 1996. USGS OF 96-532.
 Geist, E.L., Lynett, P.J., Chaytor, J.D., 2009. Hydrodynamic modeling of tsunamis from the Currituck landslide. *Mar. Geol.* 264, 41–52 (this volume).
 Hornbach, M.J., Lavier, L.L., Ruppel, C.D., 2007. Triggering mechanism and tsunamigenic potential of the Cape Fear slide complex. *G-cubed* 8 (12), Q12008. doi:10.1029/2007GC001722.
 Hughes Clarke, J.E., Shor, A.N., Piper, D.J.W., Mayer, L.A., 1990. Large-scale current-induced erosion and deposition in the path of the 1929 Grand Banks turbidity current. *Sedimentology* 37, 613–629.
 Hynes-Griffin, M.E., Franklin, A.G., 1984. Rationalizing the seismic coefficient method. U.S. Army Engineer Waterways Experiment Station Misc. pap., GL-84-13, 21 pp.
 Keefer, D.K., 1984. Landslides caused by earthquakes. *Geol. Soc. Am. Bull.* 95, 406–421.
 Keefer, D.K., 2002. Investigating landslides caused by earthquakes; a historical review. *Surv. Geophys.* 23, 473–510.
 Lee, H.J., 2009. Timing of occurrence of large submarine landslides on the Atlantic ocean margin. *Mar. Geol.* 264, 53–64.
 Lee, H.J., Locat, J., Dartnell, P., Minasian, D., Wong, F., 2000. A GIS-based regional analysis of the potential for shallow-seated submarine slope failure. *Proc. 8th Int. Sympos. on Landslides*, Cardiff, Wales, June 26–30, pp. 917–922.
 Locat, J., Desgagnes, P., Leroueil, S., Lee, H.J., 2003. Stability of the Hudson Apron slope off New Jersey. In: Locat, J., Meinert, J. (Eds.), *Submarine mass Movements and Their Consequences*. Kluwer Series on Natural and Technological Hazards. Kluwer, Dordrecht, pp. 257–270.
 Locat, J., Lee, H.J., ten Brink, U.S., Twichell, D., Geist, E., Sansoucy, M., 2009. Geomorphology, stability, and mobility of the Currituck slide. *Mar. Geol.* 264, 28–40.
 Lopez, A.M., ten Brink, U.S., Geist, E.L., 2008. Submarine landslide as the source for the 1918 Mona Passage tsunami: observations and modeling. *Mar. Geol.* 254, 35–46.
 Makdisi, F.I., Seed, H.B., 1978. Simplified procedure for estimating dam and embankment earthquake-induced deformations. *J. Geotech. Eng. Div.* 104 (GT7), 849–867.
 Mazzotti, S., Adams, J., 2005. Rates and uncertainties on seismic moment and deformation in eastern Canada. *J. Geophys. Res.* 110, B09301. doi:10.1029/2004JB003510.
 McCall, C., Morrison, M.L., Piper, D.J.W., 2005. Geological data from the St. Pierre Slope around the epicenter of the 1929 Grand Banks earthquake.
 Morgenstern, N.R., 1967. Submarine slumping and the initiation of turbidity currents. In: Richards, A.F. (Ed.), *Marine Geotechnique*. University of Illinois Press, Urbana, IL, pp. 189–210.
 Mosher, D.C., Piper, D.J.W., 2007. Analysis of multibeam seafloor imagery of the Laurentide Fan and the 1929 Grand Banks landslide area. In: Lykousis, V., Sakellariou, D., Locat, J. (Eds.), *Submarine Mass Movements and Their Consequences*. Springer, Dordrecht, pp. 77–88.
 Mosher, D.C., Moran, K., Hiscott, R.N., 1994. Late Quaternary sediment, sediment mass flow processes and slope stability on the Scotian Slope, Canada. *Sedimentology* 41, 1039–1061.
 Newmark, N.M., 1965. Effects of earthquakes on dams and embankments. *Geotechnique* 15, 139–159.
 Piper, D.J.W., Aksu, A.E., 1987. The source and origin of the 1929 Grand Banks turbidity current inferred from sediment budgets. *Geo-Mar. Lett.* 7, 177–182.
 Piper, D.J.W., Shor, A.N., Farre, J.A., O'Connell, S., Jacobi, R., 1985. Sediment slides and turbidity currents on the Laurentian Fan; sidescan sonar investigations near the epicenter of the 1929 Grand Banks earthquake. *Geology* 13, 538–541.
 Piper, D.J.W., Cochonot, P., Morrison, M.L., 1999. The sequence of events around the epicentre of the 1929 Grand Banks earthquake; initiation of debris flows and turbidity current inferred from sidescan sonar. *Sedimentology* 46, 79–97.
 Rodriguez, C.E., Bommer, J.J., Chandler, R.J., 1999. Earthquake-induced landslides: 1980–1997. *Soil Dyn. Earthq. Eng.* 18, 325–346.

- Seed, H.B., Lee, K.L., 1966. Liquefaction of saturated sands during cyclic loading. *J. Soil Mech. Found. Div., ASCE* 92 (SM6).
- Swafford, L., Stein, S., 2007. Limitations of the short earthquake record for seismicity and seismic hazard studies. In: Stein, S., Mazzotti, S. (Eds.), *Continental Intraplate Earthquakes*. Geological Society of America Special Paper, vol. 425. Geological Society of America, Boulder, pp. 49–58.
- Tappin, D.R., Watts, P., McMurtry, G.M., Lafoy, Y., Matsumoto, T., 2001. The Sissano, Papua New Guinea tsunami of July 1998; offshore evidence on the source mechanism. *Mar. Geol.* 175, 1–23.
- Tavakoli, B., Pezeshk, S., 2005. Empirical-stochastic ground-motion prediction for eastern North America. *Bull. Seismol. Soc. Am.* 95, 2283–2296.
- Travasarou, T., Bray, J.D., Abrahamson, N.A., 2003. Empirical attenuation relationship for Arias intensity. *Earthq. Eng. Struct. Dyn.* 32, 1133–1155.
- Twichell, D.C., Chaytor, J.D., ten Brink, U.S., 2009. Geologic controls on the distribution of submarine landslides along the U.S. Atlantic continental margin. *Mar. Geol.* 264, 4–15.
- Weber, K.M., List, J.H., Morgan, K.L.M., 2005. An operational mean high water datum for determination of shoreline position from topographic lidar data. USGS OF 2005-1027.
- Wells, D.L., Coppersmith, K.J., 1994. New empirical relationships among magnitude, rupture length, rupture width, rupture area, and surface displacement. *Bull. Seismol. Soc. Am.* 84, 974–1002.